Molecular Cell, Vol. 15, 375–388, August 13, 2004, Copyright ©2004 by Cell Press

Visualizing a Circadian Clock Protein: Crystal Structure of KaiC and Functional Insights

Rekha Pattanayek,[1,4] Jimin Wang,[2,4] Tetsuya Mori,[3] Yao Xu,[3] Carl Hirschie Johnson,[3,*] and Martin Egli[1,*]
[1]Department of Biochemistry
Vanderbilt University
Nashville, Tennessee 37232
[2]Department of Molecular Biophysics and Biochemistry
Bass Center for Structural Biology
New Haven, Connecticut 06520
[3]Department of Biological Sciences
Vanderbilt University
Nashville, Tennessee 37235

Summary

Circadian (daily) biological clocks express characteristics that are difficult to explain by known biochemical mechanisms, and will ultimately require characterizing the structures, functions, and interactions of their molecular components. KaiC is an essential circadian protein in cyanobacteria that forms the core of the KaiABC clock protein complex. We report the crystal structure of the KaiC homohexameric complex at 2.8 Å resolution. The structure resembles a double doughnut with a central pore that is partially sealed at one end. The crystal structure reveals ATP binding, intersubunit organization, a scaffold for Kai-protein complex formation, the location of critical KaiC mutations, and evolutionary relationships to other proteins. A key auto-phosphorylation site on KaiC (T432) is identified from the crystal structure, and mutation of this residue abolishes circadian rhythmicity. The crystal structure of KaiC will be essential for understanding this circadian clockwork and for establishing its links to global gene expression.

Introduction

Circadian clocks are self-sustained biochemical oscillators. Their properties include temperature compensation, a time constant of approximately 24 hr, and high precision (Dunlap et al., 2004). These properties are difficult to explain by known biochemical reactions. The ultimate explanation for the mechanism of these unusual oscillators will require characterizing the structures, functions, and interactions of the molecular components of circadian clocks. We here analyze the components of the biological clock in the simplest cells that are known to exhibit circadian phenomena, the prokaryotic cyanobacteria, where genetic/biochemical studies have been productive (Kondo et al., 1993; Ishiura et al., 1998; Ditty et al., 2003; Nakahira et al., 2004; Johnson, 2004).

An intriguing feature of the circadian clock system of cyanobacteria is that of global gene regulation-essentially all the promoters in the organism are under circadian control (Liu et al., 1995; Johnson, 2004). Even heterologous promoters are expressed rhythmically when introduced into cyanobacteria (Katayama et al., 1999; Nakahira et al., 2004). A mutational analysis discovered that this system is regulated by at least three essential clock genes, *kaiA*, *kaiB*, and *kaiC*, that form a cluster on the chromosome (Ishiura et al., 1998). The proteins encoded by these genes interact with each other (Iwasaki et al., 1999; Taniguchi et al., 2001) to form large complexes in vivo in which KaiC is the core (Kageyama et al., 2003).

Not only do these three clock proteins interact, they influence each other's activity. KaiC appears to be the central protein; it can exist in both phosphorylated and non-phosphorylated forms in vivo (Nishiwaki et al., 2000; Iwasaki et al., 2002; Xu et al., 2003), and its phosphorylation status is correlated with clock speed in vivo (Xu et al., 2003). KaiC can auto-phosphorylate and auto-dephosphorylate in vitro (Nishiwaki et al., 2000; Xu et al., 2003). KaiA and KaiB modulate the phosphorylation status of KaiC in vitro and in vivo: KaiA enhances KaiC phosphorylation (and/or inhibits its dephosphorylation), while KaiB antagonizes the effects of KaiA (Iwasaki et al., 2002; Williams et al., 2002; Kitayama et al., 2003; Xu et al., 2003). The addition of ATP to purified KaiC in vitro initiates KaiC phosphorylation and it also stimulates the formation of hexameric KaiC ring complexes (Mori et al., 2002; Hayashi et al., 2003), which is consistent with the observation of KaiC in high molecular weight complexes in vivo (Kageyama et al., 2003).

The *kaiC* gene is an internally duplicated version of a *recA/dnaB*-like gene (Iwasaki et al., 1999; Leipe et al., 2000). RecA is a DNA recombinase and DnaB is a DNA helicase, so the similarity among RecA, DnaB, and KaiC implies that KaiC might also act upon DNA. Indeed, KaiC binds DNA substrates (Mori et al., 2002). The half-sites of KaiC, termed KaiCI and KaiCII respectively, contain shared regions that include Walker A (P loop) and B motifs involved in ATP binding and hydrolysis. KaiC contains a conserved glutamate (E78 and E318 in the CI and CII halves, respectively) that has been proposed–based on the structure of RecA–to activate the water nucleophile for in-line attack of the ATP γ-phosphate (Story et al., 1992; Leipe et al., 2000). RecA forms helical filaments (Story et al., 1992; VanLoock et al., 2003), but also hexameric ring structures of unknown function (Yu and Egelman, 1997).

We have determined the crystal structure of the core protein of the circadian clock system from *Synechococcus elongatus*, the KaiC homohexamer, at 2.8 Å resolution. The structure resembles a double doughnut with twelve ATP molecules bound at the interfaces between subunits. The KaiCI and KaiCII domains of each subunit adopt similar conformations, but their ATP binding pockets exhibit significant differences that are of functional importance. Previously identified mutations that affect rhythmicity map to the subunit interface and KaiA binding regions. The KaiC structure reveals the existence of two separate KaiA binding regions, one mapping to the waist between CI and CII, the other to the

*Correspondence: martin.egli@vanderbilt.edu (M.E.), carl.h.johnson@vanderbilt.edu (C.H.J.)
[4]These authors contributed equally to this work.

Table 1. Crystal Data, Data Collection, and Phasing and Refinement Statistics

	Tantalum Data	Native Data
Crystal Data		
Space group	$P2_12_12_1$	$P2_12_12_1$
Unit cell parameters (Å) a =	132.10	132.87
b =	134.93	135.58
c =	204.64	204.95
Wavelength (Å)	1.25500	0.97914
Resolution (Å)	50.0-3.8 (3.94-3.8)[a]	30.0-2.8 (2.9-2.8)
Unique reflections	69,919 (6,988)	87,750 (8,637)
Redundancy	7.6	9
Completeness (%)	100.0 (100.0)	99.6 (99.3)
R-merge[b]	0.077 (0.503)	0.043 (0.501)
I/sigma(I)	32.0 (0.7)	20.6 (2.2)
Phasing statistics		
Figure of merit[c]:		
All	0.31	
Centric	0.41	
Acentric	0.30	
Figure of merit[d]:		
All	0.55	
Centric	0.63	
Acentric	0.54	
Refinement statistics		
Number of:		
Protein atoms		22,958
ATP atoms		132
Water molecules		72
R-factor (%)		0.24 (0.41)
R-free (%)		0.28 (0.41)
R.m.s. deviations from ideal:		
Bond lengths (Å)		0.009
Bond angles (°)		1.36
Avg. B-factor (CI domain; Å^2)		55
Avg. B-factor (CII domain; Å^2)		70

[a] Numbers in parentheses refer to the last resolution shell.
[b] R-merge = $\Sigma_{hkl}\Sigma_i|I(hkl)_i - \langle I(hkl)\rangle|/\Sigma_{hkl}\Sigma_i\langle I(hkl)_i\rangle$ over i observations of a reflection hkl.
[c] prior to density modification
[d] after density modification

dome-shaped surface presented by the CII hexamer. The 3D-structure of KaiC is consistent with the predicted homology between KaiC half-sites and the RecA/DnaB family of recombinases/helicases based on sequence alignments (Leipe et al., 2000). Finally, the structure also sheds light on the mechanism of auto-phosphorylation by KaiC, namely the γ-phosphate of ATP from one CII subunit is transferred to T432 located on the adjacent subunit. The significance of the T432 site is confirmed by the loss of rhythmicity in a T432A mutant.

Results and Discussion

Structure Determination

The full-length KaiC protein from *Synechococcus elongatus* PCC 7942 comprising 519 amino acids and a C-terminal $(His)_6$-tag (Ishiura et al., 1998) was overexpressed in *E. coli* and crystallized from sodium formate. The protein was purified in the presence of ATP, but prior to crystallization ATP was replaced by ATPγS, a slowly hydrolyzing analog of ATP. Gel electrophoretic analyses indicate that the protein is a mixture of phosphorylated and non-phosphorylated forms. The asymmetric unit of the crystals contains a single hexameric KaiC complex of molecular weight 360 kDa with 12 molecules of ATPγS bound and the solvent content is approximately 50%. Initial phases were obtained via the single isomorphous replacement (SIR) technique at 5 Å resolution using a crystal derivatized with a Ta_6Br_{12} cluster. The heavy atom cluster bound at the 6-fold non-crystallographic symmetry axis provided accurate matrices for initial averaging and then determination of solvent boundary. Phases were extended to 2.8 Å resolution stepwise, and the entire structure was readily built into these averaged maps. The symmetry restraints were gradually released during refinement and the final refinement cycles were conducted with six individual unrestrained KaiC molecules. The current model comprises residues 14 to 497 of six subunits and has been refined to an R-factor of 24.1% (R-free 28.4%) for data between 2.8 and 30 Å resolution. Selected data collection, phasing, and refinement parameters are summarized in Table 1. The secondary structure of KaiC aligned with the sequence is shown in Figure S1 and an example of the quality of the final Fourier sum electron density is depicted in Figure S2 (see Supplemental Data at http://www.molecule.org/cgi/content/full/15/3/375/DC1/).

Overall Structures of the Hexamer and the Monomer

The overall shape of the complex (M_r approximately 360 kDa) resembles a double doughnut with a height and a

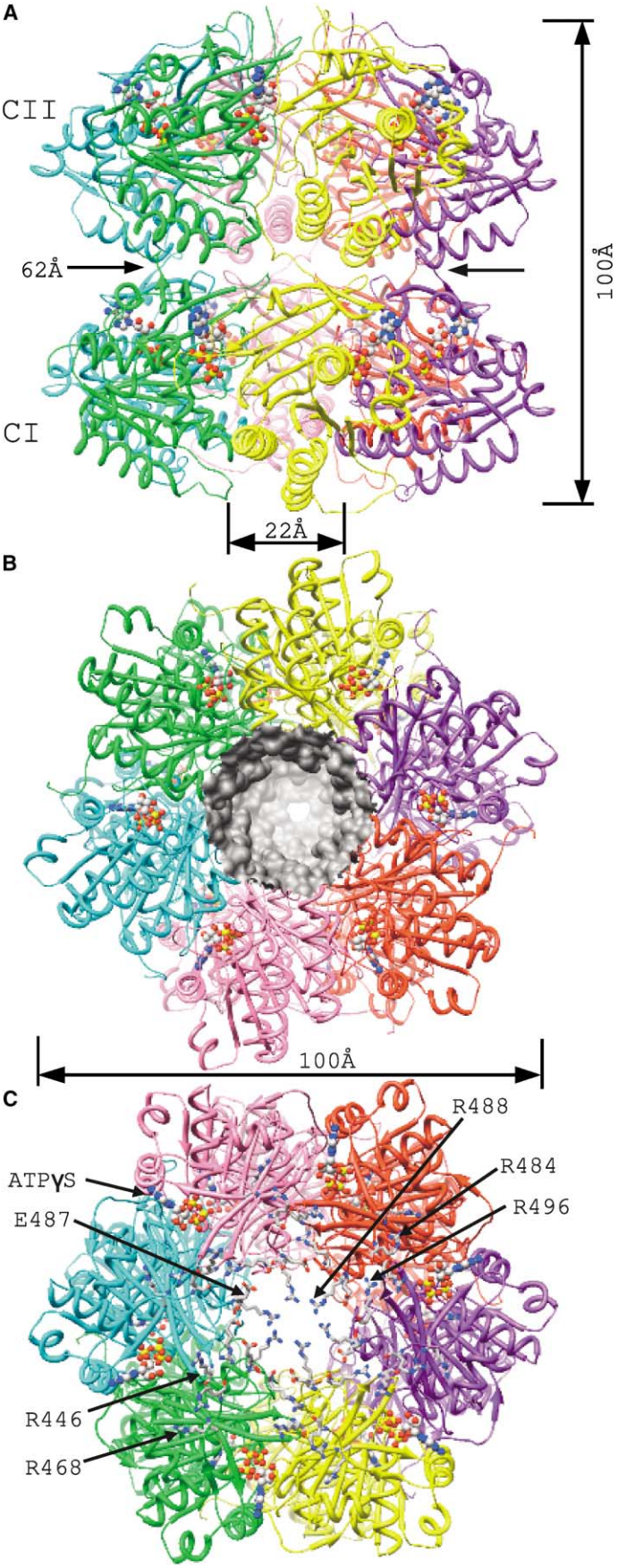

Figure 1. Overall Structure of KaiC Hexamer

(A) The hexamer complex viewed from the side, approximately perpendicular to the non-crystallographic 6-fold rotation axis (Chimera: Huang et al., 1996; Sanner et al., 1996). Individual subunits are colored differently and CI and CII domains are labeled. The slimmer waist region of the particle demarcates the CI and CII halves that are connected by a 13-residue linker. ATPγS molecules are drawn in a ball-and-stick mode with atoms colored gray, red, blue, and yellow for carbon, oxygen, nitrogen, and phosphorus, respectively.

(B) Axial view of the KaiC hexamer from the N-terminal CI side, revealing the wider end of the channel. The dimensions of the channel are illustrated by the gray inner surface of the KaiC hexamer. The CI and CII lobes are shifted laterally relative to one another, resulting in a slight inclination of KaiC monomers relative to the 6-fold rotation axis.

(C) The hexamer viewed from the C-terminal CII side, demonstrating a narrow central pore virtually sealed by six arginine residues (R488). Selected arginines and E487 protruding from the CII dome surface are labeled.

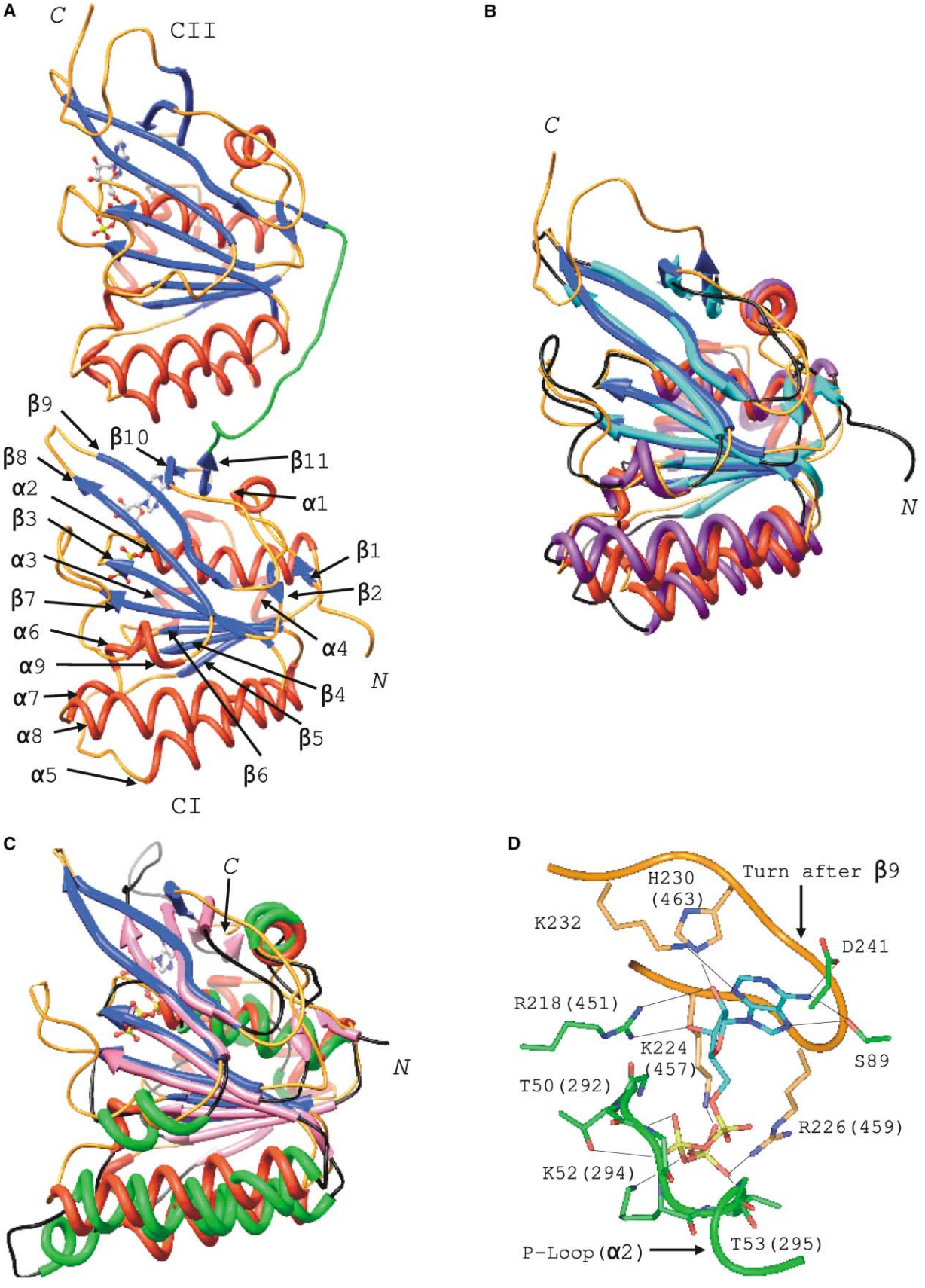
A
C
CII
β9
β10
β11
β8
α2
α1
β3
β1
α3
β2
β7
α4
α6
α9
N
β4
α7
β5
α8
β6
α5
CI
B
C
N
C
N
D
H230
(463)
Turn after β9
K232
D241
R218(451)
K224
(457)
S89
T50(292)
R226(459)
K52(294)
P-Loop(α2)
T53(295)

diameter of ca. 100 Å (Figure 1A). The subunits generate a central channel that runs all the way through. It is relatively wide and open at the N-terminal ends, narrower for part of the CII half and virtually plugged at the C-terminal ends by six arginine residues (R488; Figures 1B and 1C). Electron density sufficient to accommodate the 21 C-terminal residues (T498 to S519) is visible but not of sufficient quality to allow building of a model. However, the structure trapped in the crystal is consistent with EM reconstructions of the KaiC hexamer particle that revealed a pot-shaped structure with a sealed base (Hayashi et al., 2003). The disorder of the C-terminal region of KaiC subunits indicates that this region, and perhaps adjacent segments comprising residues that make up a cone-shaped entry to the channel on the CII surface, could adopt different conformations, e.g., opening and closing of the channel.

The core domains of both CI and CII encompass about 245 residues that adopt similar folds (Figures 2A and 2B). The turn between β5 and α5 constitutes the only region with significant conformational deviations between the CI and CII domains (Figure 2B), consistent with deletions in that region of CII (Figure S1). Their folds resemble that of the central domain of *E. coli* RecA protein (Story et al., 1992) (Figure 2C). A mostly parallel-stranded, twisted β sheet consisting of seven strands is surrounded by eight α helices. The nucleotide binding site is localized on the carboxy side of the β sheet with the triphosphate moiety bound adjacent to the amino terminus of α2 and surrounded by the P loop harboring the conserved lysine (Figures 2A and 2D). The linker between CI and CII emerges at the "waist" of the hexamer particle (Figures 1 and 2A; the interface between the CI and CII doughnuts) and winds up the outer surface of the double doughnut, eventually connecting to the β1 strand of CII (see Figure 4A, thin green upward extension of yellow C_{KABD1}).

ATP Binding and Subunit Interface

Twelve ATPγS molecules are wedged between individual subunits in both the CI and CII halves (Figure 1). In the CI half key contacts to ATP by residues from one monomer include conserved amino acids in the P loop (T50, K52, T53) as well as S89, K232 and D241 to the nucleobase (Figure 2D). Residues from the second monomer stabilizing the ATP ligand include a lysine-arginine pair (K224, R226) that contacts the γ-phosphate group and H230 hydrogen bonding to the 2′-hydroxyl group of the ribose moiety. This binding mode is consistent with the observation that lysine in the KaiCI P loop is indispensable for ATP binding (Nishiwaki et al., 2000). Moreover, it explains the strong preference for ATP over GTP by KaiCI. However, the interactions between KaiCI residues and the nucleobase moiety are not mirrored in the CII half where no direct interactions between amino acid side chains and adenine are found. This explains the reduced discrimination between ATP and GTP by KaiCII compared with KaiCI (Nishiwaki et al., 2000). Moreover, mutation of the P loop lysine corresponding to K52 in the CII half (K294H [Nishiwaki et al., 2000]) resulted in a long-period phenotype, whereas the KaiCI K52H mutant causes complete disruption of the rhythm. This is consistent with the observation that K294 does not engage in a direct contact to the γ-phosphate of ATP in the crystal structure. Another lysine (K457) forms a salt bridge to the γ-phosphate group in KaiCII (Figure 5A). Conversely, Walker A threonines form critical contacts to the γ-phosphate of ATP (via a coordinated Mg^{2+} in the case of T295 in CII) in both halves, providing an explanation for the loss of rhythm by T53A and T295A mutants (Mori and Johnson, 2001).

The crystal structure establishes clear differences between the CI and CII halves in terms of ATP binding. The KaiCI binding mode is specific for ATP's nucleobase but the structure reveals a somewhat loosely bound γ-phosphate group with a conformational disorder apparent in the electron density maps. By comparison, in KaiCII the nucleobase portion of ATP is weakly bound whereas the γ-phosphate is in a tight grip by surrounding residues and Mg^{2+} (Figure 5A). In both the KaiCI and KaiCII rings ATP molecules are almost completely sealed inside the dimer interface with the base portion accessible in part through a cleft in the CI and CII surfaces (Figure 3A).

Mapping of Mutations-KaiC Hexamer Subunit Interface

The crystal structure of KaiC offers important insights into the intramolecular (intra-hexamer) and intermolecular interactions of KaiC. In terms of intramolecular interactions, the observation described above that ATP bridges across subunits accounts for the requirement of ATP in the hexamerization and stability of KaiC (Mori et al., 2002; Hayashi et al. 2003; see Supplemental Data). An electrostatic analysis of the KaiC monomer reveals a highly hydrophilic interface by which subunits associate (Figure 3B). Interestingly, the ATP binding pockets in the CI and CII halves exhibit somewhat different electrostatic potential distributions, with the positively charged region in CII covering a more extensive surface compared to the CI half. This is in line with the above interpretation that the ATP binding modes in the two domains

Figure 2. Structures of the KaiC Monomer and the CI and CII Domains; ATP Binding

(A) Fold of the KaiC monomer. Individual α helices (red) and β strands (blue) are labeled in the CI domain and the central linker (residues 248 to 260) is highlighted in green. The color code of ATP is identical to that in Figure 1.

(B) The superposition of the KaiCI (residues 14 to 247; α helices, β strands, and loops colored in purple, cyan, and black, respectively) and KaiCII domains (residues 261 to 497; color code identical to [A]) manifests very similar folds. The overall r.m.s deviation based on 208 matching C_α pairs amounts to 2.45 Å.

(C) Superposition of the KaiCII domain (residues 262-477; color code identical to [A]) and the central domain of *E. coli* RecA (PDB code 1G19; residues 39-269; α helices, β strands, and loops colored in green, pink and black, respectively) (Story et al., 1992; Leipe et al., 2000), demonstrating the similar folds (the r.m.s. deviation for C_α pairs amounts to 1.3 Å).

(D) The ATP binding site in the CI domain. Amino acids from the A and B subunits are colored in green and orange, respectively, and are labeled. Selected hydrogen bonds are drawn with thin solid lines and corresponding residues in the CII domain forming analogous hydrogen bonds are shown in parentheses.

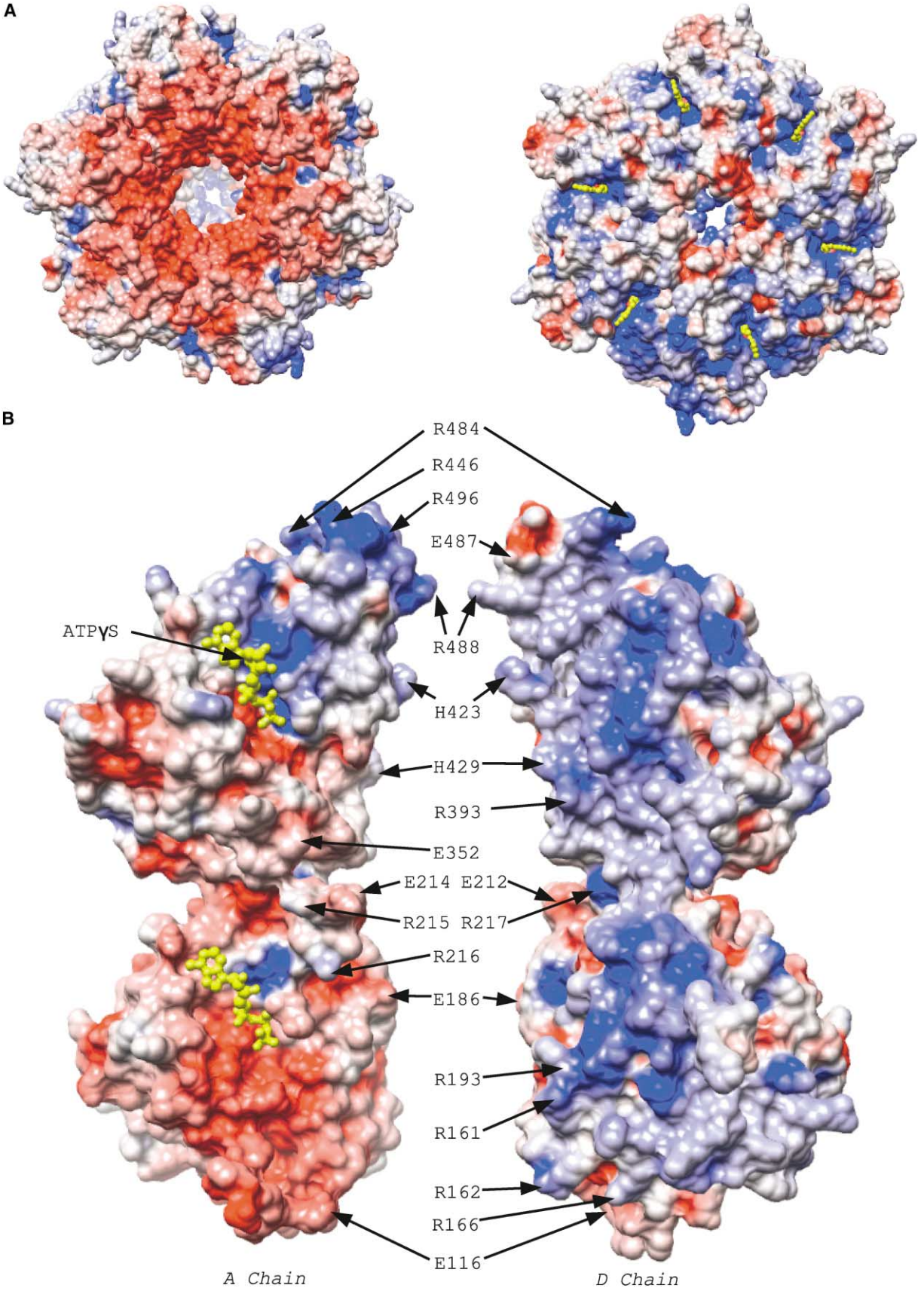
A
B
R484
R446
R496
E487
ATPγS
R488
H423
H429
R393
E352
E214 E212
R215 R217
R216
E186
R193
R161
R162
R166
E116
A Chain
D Chain

differ, perhaps reflecting different functions of the CI and CII rings and the ATPs bound there. Mutational analyses of circadian phenomena in cyanobacteria discovered a number of point mutations in KaiC that alter the period or abolish rhythmicity altogether (Ishiura et al., 1998; Xu et al., 2003). For example, the G460E mutation causes arhythmicity; inspection of the structure reveals that G460 is located directly at the interface between subunits and faces the nucleobase in the ATP binding pocket (Figure 4A). Introduction of a glutamate at that site is likely to sterically interfere with interactions between R326 from the same KaiC molecule and S258 and S259 from the neighboring subunit.

KaiA-KaiC Interactions

In terms of intermolecular interactions, KaiC interacts with another essential clock protein, KaiA (Iwasaki et al., 1999; Taniguchi et al., 2001). KaiA stabilizes the phosphorylation status of KaiC (Iwasaki et al., 2002; Williams et al., 2002; Kitayama et al., 2003; Xu et al. 2003), which is an important determinant of circadian period (Xu et al., 2003). A yeast two-hybrid analysis identified mutations that disrupt KaiC-KaiA interaction and KaiC domain fragments that exhibit binding to KaiA (Taniguchi et al., 2001). The KaiA binding domains in KaiC (C_{KABD1} and C_{KABD2}) were predicted by the two-hybrid analyses to be localized only to a single region, namely the interface between the CI and CII domains (Taniguchi et al., 2001), that we now know to form the waist.

The KaiA protein is composed of two domains, an N-terminal pseudo-receiver domain, similar to those present in bacterial response regulators, and the C-terminal dimerization and KaiC-interacting domain (Vakonakis et al. 2004). Vakonakis and coworkers deduced from NMR and EM studies of KaiA and KaiC that the C-terminal domain of a KaiA dimer inserts into the waist region of KaiC that links CI with CII (Vakonakis et al., 2004). Thus, the hypotheses of both Taniguchi et al. (2001) and Vakonakis et al. (2004) are consistent with binding of KaiA to the KaiC waist. However, the 3-D structure of KaiC clearly reveals that KaiA-interacting regions as well as individual mutations affecting KaiA-KaiC binding map to both the KaiCI and the KaiCII lobes (Figure 4A). The head-to-tail orientation between CI and CII hexamer rings implies that KaiA protein modulates KaiC phosphorylation by interacting with CI and CII portions that occupy distant areas on the surface of the KaiC hexamer. Knowledge of the KaiC structure allows a refined prediction of the mode and sites of interaction between KaiA and the KaiCI and KaiCII domains. The putative binding interfaces on both KaiA and KaiC are highlighted in yellow in Figure 4A (the linker highlighted in green is part of C_{KABD1}).

Figure 4B depicts dimers of the C-terminal KaiA domain opposite both the C_{KABD1} and C_{KABD2} interfaces. The convex surfaces presented by C_{KABD1} in the waist and linker regions of KaiCI and C_{KABD2} near the dome of the KaiCII domain match the concave surface (site of numerous conserved residues; data not shown) in KaiA. Moreover, the concave surface on the KaiA dimer, the region that is presumably important for KaiC binding, exhibits a mostly negative (red) electrostatic potential, while the electrostatic surface potential in the region of C_{KABD1} and C_{KABD2} is predominantly positive (Figure 4B). The modeled interactions between 2 KaiA dimers and the C_{KABD1} and C_{KABD2} regions of a single KaiC hexamer are consistent with the recent determination of the stoichiometry of KaiA-KaiC interactions (Hayashi et al., 2004). Accordingly, 2 molecules of KaiA dimer can interact with 1 molecule of KaiC hexamer. In addition it was found that interactions between 1 KaiA dimer and 1 KaiC hexamer are sufficient to increase phosphorylation of KaiC by KaiA to an almost saturated level (Hayashi et al. 2004).

Among the individual KaiC clock mutations that alter KaiA-C_{KABD} interactions (Taniguchi et al., 2001), Y442H that generates a long period (60 hr) is particularly intriguing since it is located in the immediate vicinity of the ATP binding site and near the surface (Figure 4A). Therefore, binding of KaiA to KaiC may seal clefts that mark the nucleotide binding pockets on the CII dome surface and at the CI waist (Figure 3A; shown only for CII). KaiA's protection of the ATP binding site could prolong the residence time of ATP, thereby explaining KaiA's enhancement of KaiC auto-phosphorylation (Iwasaki et al., 2002; Williams et al., 2002) and inhibition of KaiC autodephosphorylation (Xu et al., 2003). At present it is unclear if KaiA-KaiC binding is cooperative, i.e., whether binding of one KaiA molecule to the KaiC hexamer enhances binding of a second one. It is remarkable that one of the KaiC subunits exhibits an electrostatic surface potential in the C_{KABD2} region that is considerably different from the other five (Figure 3A; blue patch at bottom of right panel). The more positive polarization at that site is not a consequence of an obvious conformational difference in the subunit. It is clear that a more detailed understanding of the KaiA-KaiC interactions will ultimately require the determination of crystal structures of complexes.

KaiB antagonizes the action of KaiA (Iwasaki et al., 2002; Williams et al., 2002; Kitayama et al., 2003; Xu et al., 2003), and the crystal structures of KaiB along with that of KaiA from the cyanobacteria *Anabaena* have recently been published (Garces et al., 2004). Based on

Figure 3. Electrostatics of KaiC and Subunit Interface

(A) Electrostatic surface representation (GRASP, Nicholls et al., 1993) of KaiC viewed from the CI side (left). Full charges were used at all Asp, Glu, Arg, and Lys residues and half charge at all His residues and the energy range is between –16 and +16 k_BT/e. Note the mostly negative (red) potential around the channel opening and inside the CI portion of the channel. Electrostatic surface representation of KaiC viewed from the CII side (right). Note the mostly positive (blue) potential of the area that covers the predicted KaiA binding domain (C_{KABD2}; Taniguchi et al., 2001). ATP molecules are highlighted in yellow to accentuate the proximity of the adenine moieties to the protein surface.

(B) Electrostatic surface representations for two KaiC subunits opposing each other in the hexamer complex reveal the strongly hydrophilic hexamerization interface. The orientation of subunit D (right) is similar to that in Figure 2A and rotated 180 degrees around the vertical relative to subunit A on the left. ATP molecules are highlighted in yellow and the CI and CII domains and charged residues lining the channel and the openings at both ends are labeled.

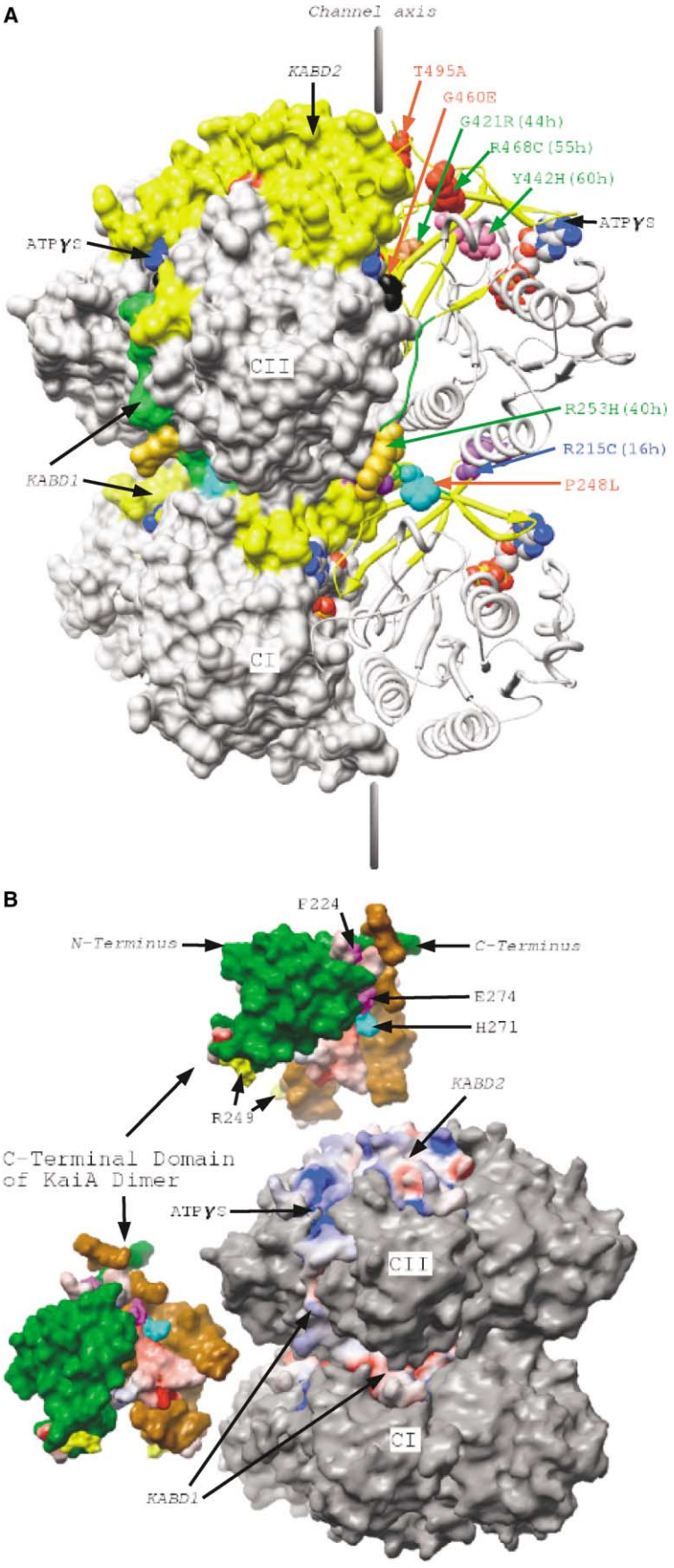

Figure 4. Mapping of Mutations and KaiA-KaiC Interactions

(A) Mapping of KaiC mutations that affect KaiA-KaiC interactions and circadian phenotypes. Two subunits of KaiC are shown in a surface representation and one additional subunit is represented with a ribbon diagram. KaiA binding domains of KaiC based on a deletion and yeast two-hybrid analysis (Taniguchi et al., 2001); C_{KABD1} (residues 206-263) and C_{KABD2} (residues 418-519) are colored in yellow and the central linker that was included in C_{KABD1} (residues 248 to 261) is highlighted in green. Individual mutations are highlighted in CPK mode and are labeled in red (arhythmic), green (long period), or blue (short period). The mutations shown include five individual mutations within either C_{KABD1} or C_{KABD2} (R215C, P248L, G421R, Y442H, and T495A) that were shown to significantly affect KaiA-KaiC interaction (Taniguchi et al., 2001). Further, two mutations, one affecting the length of the period (R253H) and the other eliciting arhythmicity (G460E), map to the waist region and the subunit interface in immediate vicinity of bound ATP, respectively. The R468C mutant has a very long period (Xu et al., 2003) and most likely affects KaiA-KaiC interaction as it maps to C_{KABD2}.

(B) Two dimers of the C-terminal KaiA domain (model based on the NMR solution structure; Vakonakis et al., 2004) positioned opposite their putative KaiC binding interfaces (labeled). KaiA monomers are colored in green and beige. The likely site for binding to KaiC on KaiA is a concave surface harboring more than 20 residues that are conserved between various strains (highlighted by its electrostatic surface potential). Residue H271 (residue numbers refer to KaiA from *Synechococcus elongatus*), located in the center of the concave surface, is highlighted in cyan and is important for the functional interaction with KaiC (Hayashi et al., 2004; Uzumaki et al., 2004). Residues E274 and F224 that alter *KaiBC* expression when mutated to S and K, respectively (Garces et al., 2004, and cited references) are highlighted in magenta. These mutations likely alter the KaiA dimer interface (Uzumaki et al., 2004; Ye et al., 2004). Residue R248 is highlighted in yellow; mutation of the equivalent residue (R69A) in *Anabaena* resulted in a drastic loss of binding affinity between KaiA and KaiC (Garces et al., 2004). The figure also depicts the electrostatic surface potentials of the C_{KABD1} and C_{KABD2} regions on KaiC, highlighted in yellow in Figure 4A). The convex shapes presented by C_{KABD1} and C_{KABD2} are compatible with the concave surface of the putative binding region in KaiA. Moreover, the electrostatic surface potentials of C_{KABD1} and C_{KABD2} (mostly positive = blue), particularly in the case of one subunit (see Figure 3A, right), and of the concave binding region in KaiA (mostly negative = red) are complementary. The electrostatic surface representations were computed with the program GRASP (Nicholls et al., 1993). Full charges were used at all Asp, Glu, Arg, and Lys residues and half charge at all His residues and the energy range is between −16 and +16 k_BT/e.

these structures the authors propose that KaiA and KaiB could compete for a common binding site on KaiC. A different model for KaiB's action was put forth based on the recently determined crystal structure of full-length KaiA from *Synechococcus elongatus* (Ye et al., 2004). In the crystal the KaiA dimer exhibits a closed conformation with intricate interactions between the N-terminal receiver domain from one monomer and the C-terminal KaiC binding domain from the other. Detaching the N-terminal receiver domain may open the KaiB binding site on the C-terminal domain, thus allowing KaiB to antagonize KaiA's action by directly binding to it (Ye et al., 2004). Such models represent the beginning of our understanding how KaiB might antagonize KaiA action, but they leave open the question regarding the precise interactions between KaiB (bound to KaiA or free) and KaiC.

Structure-Based Identification of a KaiC Auto-Phosphorylation Site

KaiC's phosphorylation status is correlated with clock speed in vivo (Xu et al., 2003). Although KaiC is known to auto-phosphorylate and auto-dephosphorylate in vitro (Nishiwaki et al., 2000; Xu et al. 2003), it has not been possible to determine the identity of the phosphorylated amino acids. This auto-phosphorylation involves threonine and serine residues in a 2:1 ratio and KaiA can enhance KaiC phosphorylation without altering the ratio (Iwasaki et al., 2002). We inspected difference (F_o-F_c) Fourier electron density maps computed at different thresholds to find out whether threonines or serines situated within an 8-Å radius sphere centered at the γ-phosphate group in any of the six subunits displayed residual density around their hydroxyl groups, potentially indicating presence of a partially or fully occupied phosphate. The expectation to locate phosphorylated threonine and/or serine residues in electron density maps was based on the fact that ATP had been present throughout protein purification, resulting in a mixture of phosphorylated and unphosphorylated KaiC molecules prior to crystallization. ATP was replaced by ATPγS just before the crystallization experiments. In KaiCI, the T48, T50, T53, S89, S146, and T181 residues lie fully or partly inside the 8-Å sphere (Figure S1). T53 and S89 both form a hydrogen bond to ATP (Figure 2D) and none of the other residues exhibited any significant difference density. Threonines and serines within 8 Å from the γ-phosphate in KaiCII include residues T290, T292, T295, T415, S431, T432, and T434.

Both T290 and T295 are part of the P loop and were not considered as candidates for auto-phosphorylation. However, this analysis found additional electron density (at the 4σ level) within a distance of $<$2 Å for T432 in all six subunits (Figure 5A). Other 4σ difference electron density peaks can be attributed to Mg^{2+} displaying inner-sphere coordination to the γ-phosphate. In addition, the metal ion coordinates to residues E318, E319, D378, and T295, either via the inner- or outer-sphere mode. The carboxylate of E318 lies within hydrogen bonding distance from the hydroxyl group of T432 and could potentially activate the latter for nucleophilic attack at the γ-phosphate. The metal ion and residues K457 and K294 are likely involved in transition state and leaving group stabilization of the phosphoryl transfer reaction. These observations establish T432 as a primary candidate for auto-phosphorylation by KaiC. This residue is highly conserved in cyanobacteria based on an alignment of KaiC sequences from multiple species (data not shown).

Structure-Directed Generation of a Key KaiC Mutant

In the first example of using a three-dimensional structure to guide mutagenesis of a circadian clock protein, we generated a T432A mutation in KaiC by site-directed mutagenesis. $KaiC_{T432A}$ was inserted into a KaiC deletion strain under the control of the derepressible promoter *trc*p as described previously (Xu et al., 2003). The use of *trc*p allows the expression of proteins at various levels of expression by modulating the concentration in the medium of the inducer IPTG. The KaiC deletion strain is arhythmic (Xu et al., 2003), but when wild-type $KaiC_{WT}$ is inserted into this strain, rhythmicity is restored at low levels of expression (0-8 μM IPTG), as shown in Figure 5B (Xu et al., 2003). High levels of expression of $KaiC_{WT}$ repress rhythmicity (32 μM IPTG, Figure 5B), as shown previously (Ishiura et al., 1998; Xu et al., 2003). In contrast, expression of $KaiC_{T432A}$ will not allow rhythmicity at any expression level (Figure 5B). Because alanine residues cannot be phosphorylated, this result confirms that a phosphorylatable threonine residue at position 432 of KaiC is required for proper operation of the circadian clock in cyanobacteria.

Structural and Evolutionary Relationships

KaiCI and KaiCII are members of the DnaB/RecA superfamily (Leipe et al., 2000). The earlier evidence based on sequence comparisons is clearly borne out by the 3D-structure. Structural comparisons using the DALI suite conducted with either the CI or CII domain provided evidence for these relations (Holm and Sanders, 1998). In addition to RecA, these comparisons revealed similarities between KaiC and hexameric ring-shaped ATPases containing Walker A and B motifs, such as various DNA helicases (Egelman, 1998) and DNA pumps (i.e., TrwB) (Gomis-Rüth et al., 2001). Another structural relation exists to proteins that do not bind DNA, such as F1-ATPase (Abrahams et al., 1994). A three-dimensional structural alignment between the KaiCII domain and the $\alpha3\beta3$ ring from F1-ATPase (Abrahams et al., 1994) is depicted in Figure 6A and reveals a good fit for all six subunits. The root mean square deviation (*rmsd*) amounts to 2.1 Å for 1772 Cα atoms from the CII and F1-ATPase $\alpha3\beta3$ rings. This fit is superior to the one between TrwB and F1-ATPase and KaiCII and the hexameric ring of gene 4 helicase from T7 (Singleton et al., 2000) (Figure 6B).

The structural similarities at the levels of both the hexameric rings (Figure 6B) and monomeric subunits (Figure 6C) between KaiC and various helicases suggest that the channel in KaiC may be the location where DNA is bound. The diameter of the central pore in KaiC, apart from the C-terminal end that is partly constricted by Arg488 and His 423 residues, is suitable for accommodating single-stranded DNA (Figures 1 and 3B). The electrostatic surface potential at the channel opening and inside the channel of the CI domain is mostly negative (Figure 3A). Conversely, it is mostly positive inside the

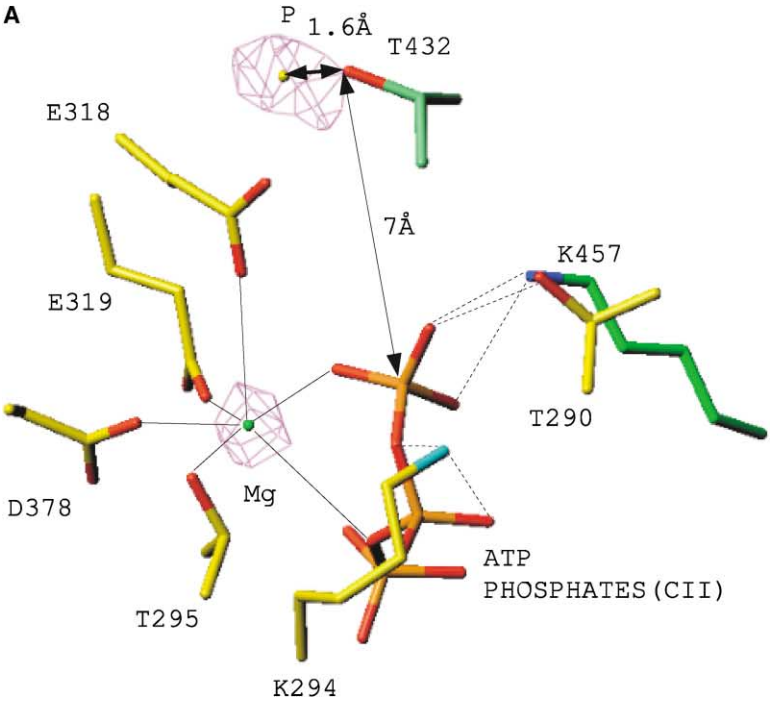

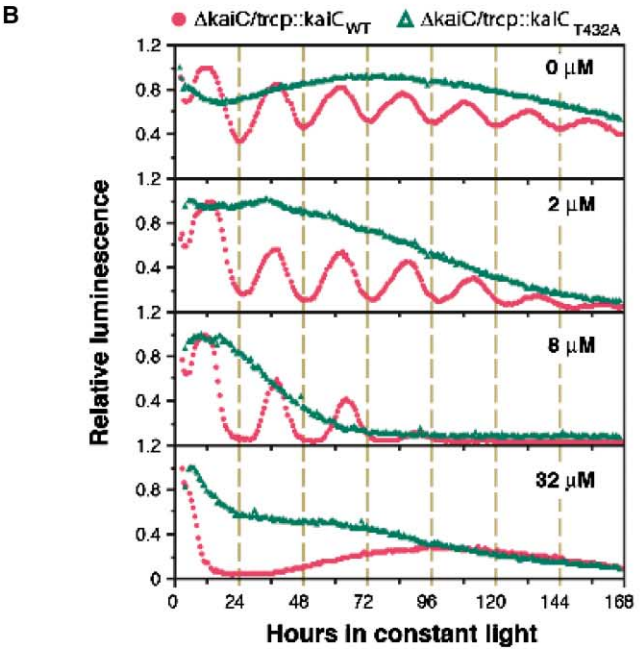

Figure 5. A Putative Auto-Phosphorylation Site in KaiCII

(A) Two regions of 4σ (F_o-F_c) difference electron density can be interpreted as Mg^{2+} and phosphate covalently bound to O_G of T432, respectively. The coordination sphere of Mg^{2+} is indicated with thin lines (note that D378 is part of the Walker B motif) and distances between O_G(T432) and γP(ATP) as well as O_G(T432) and the putative phosphate group are shown.

(B) Mutation of a putative phosphorylation residue (T432) of KaiC causes arhythmicity. The *kaiBC* promoter (*kaiBC*p) can be functionally replaced by an IPTG-derepressible heterologous promoter, *trc*p (Xu et al., 2003). Constructs with *trc*p-driving wild-type KaiC (*kaiC*$_{WT}$) or mutant KaiC (*kaiC*$_{T432A}$) expression were introduced into neutral site II of a strain in which the endogenous *kaiC* gene is deleted (Δ*kaiC*) to make the ΔkaiC/*trc*p::*kaiC*$_{WT}$ (pink) and ΔkaiC/*trc*p::*kaiC*$_{T432A}$ (green) strains, respectively. Varying the concentration of IPTG drives the expression of varying levels of KaiC expression (Xu et al., 2003). The concentration of IPTG (in μM) is shown in the upper-right corner of each panel. Circadian gene expression is monitored as luminescence of a luciferase reporter in constant light, and the maximum levels of luminescence were normalized to 1.

channel of the CII half and in the area of the C-terminal channel opening (Figure 3A), establishing a further difference between the two domains. Furthermore, it is noteworthy that the surface of the channel and the funnel-like openings in the CI and CII halves harbor a considerable number of charged residues, among them no fewer than 14 arginines and histidines (Figure 3B). Structural rearrangements may bring about changes in the dimension and the electrostatic surface potential of the channel. In this respect, it is instructive that the long-period G421R mutant affects KaiA-KaiC interaction (Taniguchi et al., 2001). Residue 421 is located inside the channel (Figure 4A) and the observation that KaiA binding is affected by its mutation implies that the channel can open up at the CII end.

Implications for KaiC's Biochemical Activity

Several independent lines of evidence suggest that global circadian gene orchestration in cyanobacteria is mediated by changes in chromosomal torsion in which KaiC plays a role as an essential clock protein (Mori and Johnson, 2001; Xu et al., 2003; Min et al., 2004; Nakahira et al., 2004; Johnson, 2004). In addition, the clear sequence (Leipe et al., 2000) and structural homologies

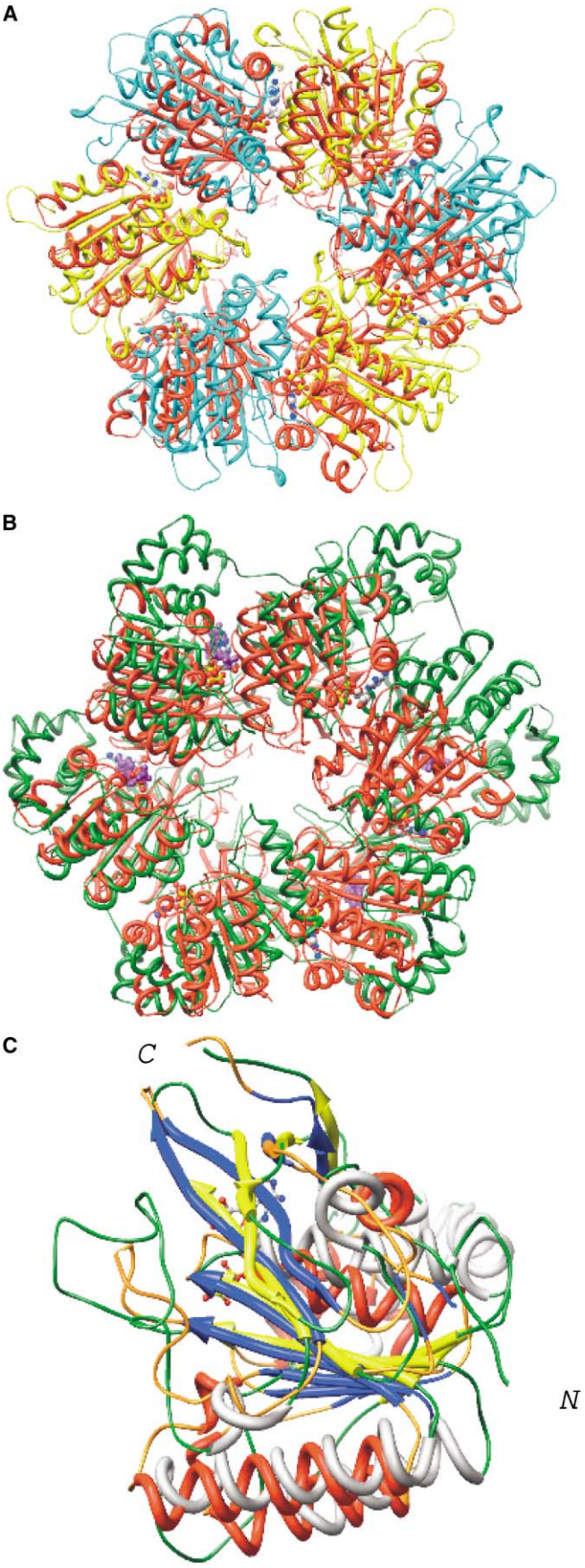

Figure 6. Relationship between the KaiC Hexamer and Other Ring-Shaped Complexes

(A) Superposition of the KaiC hexamer (red; CII ring only) and the $\alpha 3\beta 3$ ring from F1-ATPase (PDB code 1BMF) (Abrahams et al., 1994). The α and β subunits of F1-ATPase are colored cyan and yellow, respectively.

(B) Superposition of the KaiC hexamer (red; CII ring only) and the hexameric ring formed by the gene 4 helicase from bacteriophage T7 (PDB code 1E0J; green) (Singleton et al., 2000). In both panels ATPγS molecules bound to KaiCII are shown in ball-and-stick mode and four ADPNP molecules bound to the gene 4 helicase are shown in purple.

(C) Superposition of the KaiCII domain (color code identical to Figure 2A) and a monomer of T7 primase-helicase (PDB code 1Q57; α helices, β strands, and loops colored in gray, yellow, and green, respectively) (Toth et al., 2003).

between KaiC and RecA (Figure 2C) and many helicases (Figures 6B and 6C) imply that KaiC might interact directly with nucleic acids. KaiC does not appear to have significant DNA helicase activity based on several standard strand displacement and ATPase activity assays (Podust and C.H.J., unpublished data). However, it binds forked DNA substrates (but not double-stranded DNA) (Mori et al., 2002) and we have recently found that KaiC also binds single stranded DNA (T.M. and C.H.J., unpublished data). It is noteworthy that there are many helicases that have been identified on the basis of sequence and structure for which biochemical activity cannot be measured. Presumably this is because the exactly appropriate conditions and/or substrates have not been identified. Currently, there is much debate on the mechanisms of helicases (Laskey and Madine, 2003). Accordingly, some helicases may work at a DNA fork, but other helicases may work from a distance and act like a DNA "pump." Despite the negative results regarding KaiC helicase activity, the existing DNA binding data, together with the determination that there are approximately 10,000 molecules of KaiC per cell (Kitayama et al., 2003), are consistent with the hypothesis that KaiC acts to regulate global gene expression by a pervasive mechanism that may involve changes in DNA structure (Mori and Johnson, 2001; Xu et al., 2003; Nakahira et al., 2004; Johnson, 2004).

The KaiC structure presented here explains previously reported properties of KaiC (and KaiA) and offers insight into the intramolecular and intermolecular interactions of KaiC as well as the identification of key residues involved in regulating KaiC phosphorylation status and circadian period of the cyanobacterial clockwork. Along with the determination of the crystal structures of KaiA (Williams et al., 2002; Garces et al., 2004; Uzumaki et al., 2004; Vakonakis et al. 2004; Ye et al., 2004) and KaiB (Garces et al., 2004), knowledge of the KaiC structure initiates a new phase of research on biological clock mechanisms whereby the effects of mutations and molecular interactions can be more accurately predicted because they will be visualized three-dimensionally. Undoubtedly, this ability will facilitate the testing of hypotheses that attempt to explain the molecular basis of the biological clock.

Experimental Procedures

Protein Purification and Crystallization

Expression and purification of full-length KaiC protein from *Synechococcus elongatus* PCC 7942 was performed as previously described (Mori et al., 2002) and as described more fully in the Supplemental Data. In brief, the KaiC protein with hexahistidine at its carboxyl end (KaiC::His_6) was overexpressed in *E. coli* cells and purified in the presence of ATP on a metal affinity chromatography column (TALON IMAC resin, BD Biosciences Clontech), followed by gel filtration, concentration to 10~20 mg/ml, and finally by replacement of ATP in the sample buffer with ATPγS by ultrafiltration.

The concentration of the stock solution was adjusted to 8 mg/ml in 20 mM Tris•HCl buffer, pH 7.8, and 2 mM DTT. Crystallization conditions were found using the sparse matrix "Crystal Screen" by Hampton Research (Aliso Viejo, CA) (Jancarik and Kim, 1991). Crystals grew at 18°C from sodium acetate buffer using sodium formate as the precipitant and belong to space group $P2_12_12_1$ with unit cell dimensions a = 132.87, b = 135.58 and c = 204.95 Å. Selected crystal data are summarized in Table 1. The asymmetric unit contains six KaiC molecules, indicative of a hexameric particle as observed earlier in EM studies (Mori et al. 2002; Hayashi et al., 2003).

Structure Determination

For low-temperature data collection, crystals were cryoprotected in 25% glycerol and frozen in liquid nitrogen. Diffraction data to 2.8 Å resolution were collected at 0.9791 Å wavelength using a MAR225 CCD detector on the insertion device beamline of the DuPont-Northwestern-Dow Collaborative Access Team of the Advanced Photon Source (APS), Argonne, Illinois. All data were integrated and scaled with the program XDS (Kabsch, 1993) and a summary of the data quality and statistics is provided in Table 1.

For heavy-atom derivatization KaiC crystals were soaked in solutions of $Ta_6Br_{12}^{2+}$ for various durations. Crystals turned green and retained their color after back-soaking. SAD data collections were conducted at 1.26 Å wavelength using a MAR225 CCD detector on the insertion device beamline of the South-Eastern Regional Collaborative Access Team at the APS. The particular derivative crystal eventually used for phase determination initially diffracted X-rays to about 5 Å resolution, but annealing resulted in improved diffraction up to a maximum of 3.5 Å. All data were integrated and scaled with the program HKL2000 (Otwinowski & Minor, 1997) and a summary of the data quality and statistics is provided in Table 1.

The self-rotation function based on wt-KaiC data and calculated with the program GLRF (Tong and Rossmann, 1990) revealed the presence of a non-crystallographic 6-fold rotation axis oriented at approximately 30° relative to the crystallographic *c*-axis. This observation indicated that non-crystallographic symmetry (NCS) averaging would be of significant help in the phase determination of the KaiC protein complex. The anomalous difference Patterson analysis revealed a single $Ta_6Br_{12}^{2+}$ site through which the 6-fold axis passes. SIR/AS-type refinement with the program MLPHARE (CCP4, 1997) was used to generate initial experimental phases at 5 Å. Density modification with RESOLVE (Terwilliger, 1997) failed to extend the phases beyond 4.5 Å due to large errors in the NCS matrices and mask. At this point the mask was re-determined at 5 Å and the NCS matrices were manually refined at 5 Å until full convergence. With these new parameters averaging was repeated and phases were extended in steps of 0.2 Å and beyond 3.5 Å in steps of 0.1 Å up to a final resolution of 2.8 Å. The computed experimental map was of excellent quality. A model of a single KaiC subunit was built into the average density using the program O (Jones and Kjeldgaard, 1997). The initial model was refined with the program CNS (Brünger et al., 1998), using 5% (randomly chosen) of the reflections to calculate the R-free (Brünger, 1992). The partially refined model was symmetry-transformed into five additional subunits to complete the hexameric complex and the NCS restraints were switched off as refinement was continued with the full KaiC hexamer.

Along with 485 amino acids per subunit, 12 ATPγS molecules were included in the current model and a summary of the refinement parameters is provided in Table 1. An example of the quality of the final electron density map is depicted in Figure S2. The backbone angle pairs of all residues fall into allowed regions of the Ramachandran plot (analyzed with the program PROCHECK [CCP4, 1994]). The angle pairs of 87% of the residues fall into the allowed region, 11.6% are in the additionally allowed region, and the remaining 1.4% lie in the generously allowed region.

Structure Alignments

Least squares superpositions between pairs of monomers or hexameric rings were carried out with either program CHIMERA (Huang et al., 1996) or O (Jones and Kjeldgaard, 1997), using C_α coordinates of selected substructures for initial least squares fits, followed by inclusion of an increasing number of atom pairs.

Generation of $KaiC_{T432A}$ and Assay of Circadian Rhythms

To mutagenize residue 432 of KaiC from threonine to alanine, the nucleotide A at position 1294 relative to the translation start site of *kaiC* was converted to a G, resulting in the mutant KaiC (*$kaiC_{T432A}$*). Site-directed mutagenesis was performed using the QuikChange XL Site-Directed Mutagenesis system (Stratagene, La Jolla, CA). For the rhythm assay, we used our previously developed system for monitoring circadian gene expression under varying levels of

expression of the *kaiC* gene (Xu et al., 2003). Based on the fact that *kaiBC*p can be functionally replaced by an IPTG-derepressible heterologous promoter (*trc*p), *trc*p-driving wild-type KaiC ($kaiC_{WT}$), or mutant KaiC ($kaiC_{T432A}$) constructs were introduced into neutral site II (NSII) of an in-frame deletion strain of the endogenous *kaiC* gene (ΔkaiC) strain to create ΔkaiC/*trc*p::$kaiC_{WT}$ and ΔkaiC/*trc*p::$kaiC_{T432A}$ strains, respectively, by the same methods described previously (Xu et al., 2003). Luminescence rhythms that indicate circadian activity of the *kaiBC*p::luxAB reporter in neutral site I (NS I) were monitored in constant light after a 12 hr synchronizing dark pulse as described previously (Kondo et al., 1993; Xu et al., 2003).

Acknowledgments

We thank Dr. Vladimir Podust for assistance with protein purification and helicase activity assays, Drs. Zdzislaw Wawrzak and Stephen Foundling for help with X-ray data collection and processing on the 5-ID (DND-CAT) and 22-ID (SER-CAT) beamlines, respectively, at the Advanced Photon Source, Dr. Louis Messerle for a gift of tantalum bromide, Dr. Andy LiWang for sharing data prior to publication, and Sabuj Pattanayek for help with figure preparation. Support by grants from the NIH (GM67152) and NSF (MCB-9874371) to CHJ, partial support from NIH grant GM55237 to ME, a VUMC intramural discovery grant (to ME and CHJ) and from the directorship of the Center for Structural Biology at Yale University to JW is gratefully acknowledged. Use of the Advanced Photon Source was supported by the U.S. Department of Energy, Office of Science, Office of Basic Energy Sciences, under Contract No. W-31-109-Eng-38.

Received: April 3, 2004
Revised: May 26, 2004
Accepted: June 7, 2004
Published online: July 22, 2004

References

Abrahams, J.P., Leslie, A.G.W., Lutter, R., and Walker, J.E. (1994). Structure at 2.8 Å resolution of F1 ATPase from bovine heart mitochondria. Nature *370*, 621–628.

Brünger, A.T. (1992). Free R value: a novel statistical quantity for assessing the accuracy of crystal structures. Nature *355*, 472–475.

Brünger, A.T., Adams, P.D., Clore, G.M., DeLano, W.L., Gros, P., Grosse-Kunstleve, R.W., Jiang, J.S., Kuszewski, J., Nilges, M., Pannu, N.S., et al. (1998). Crystallography and NMR system: a new software suite for macromolecular structure determination. Acta Crystallogr. D Biol. Crystallogr. *54*, 905–921.

CCP4 (Collaborative Computational Project, Number 4) (1994). The CCP4 suite: programs for protein crystallography. Acta Cryst. D *50*, 760–763.

Ditty, J.L., Williams, S.B., and Golden, S.S. (2003). A cyanobacterial circadian timing mechanism. Annu. Rev. Genet. *37*, 513–543.

Dunlap, J.C., Loros, J.J., and DeCoursey, P.J. (2004). Chronobiology: Biological Timekeeping (Sunderland, MA: Sinauer).

Egelman, E.H. (1998). Bacterial helicases. J. Struct. Biol. *124*, 123–128.

Garces, R.G., Wu, N., Gillon, W., and Pai, E.F. (2004). Anabaena circadian clock proteins KaiA and KaiB reveal potential common binding site to their partner KaiC. EMBO J. *23*, 1688–1698.

Gomis-Rüth, F.X., Moncalián, G., Pérez-Luque, R., González, A., Cabezón, E., de la Cruz, F., and Coll, M. (2001). The bacterial conjugation protein TrwB resembles ring helicases and F_1-ATPase. Nature *409*, 637–641.

Hayashi, F., Suzuki, H., Iwase, R., Uzumaki, T., Miyake, A., Shen, J.-R., Imada, K., Furukawa, Y., Yonekura, K., Namba, K., and Ishiura, M. (2003). ATP-induced hexameric ring structure of the cyanobacterial circadian clock protein KaiC. Genes Cells *8*, 287–296.

Hayashi, F., Ito, H., Fujita, M., Iwase, R., Uzumaki, T., and Ishiura, M. (2004). Stoichiometric interactions between cyanobacterial clock proteins KaiA and KaiC. Biochem. Biophys. Res. Commun. *316*, 195–202.

Holm, L., and Sander, C. (1998). Touring protein fold space with Dali/FSSP. Nucleic Acids Res. *26*, 316–319.

Huang, C.C., Couch, G.S., Pettersen, E.F., and Ferrin, T.E. (1996). Chimera: an extensible molecular modeling application constructed using standard components. Pacific Symposium on Biocomputing *1*, 724.

Ishiura, M., Kutsuna, S., Aoki, S., Iwasaki, H., Andersson, C.R., Tanabe, A., Golden, S.S., Johnson, C.H., and Kondo, T. (1998). Expression of a gene cluster *kaiABC* as a circadian feedback process in cyanobacteria. Science *281*, 1519–1523.

Iwasaki, H., Taniguchi, Y., Kondo, T., and Ishiura, M. (1999). Physical interactions among circadian clock proteins, KaiA, KaiB and KaiC, in Cyanobacteria. EMBO J. *18*, 1137–1145.

Iwasaki, H., Nishiwaki, T., Kitayama, Y., Nakajima, M., and Kondo, T. (2002). KaiA-stimulated KaiC phosphorylation in circadian timing loops in cyanobacteria. Proc. Natl. Acad. Sci. USA *99*, 15788–15793.

Jancarik, J., and Kim, S.-H. (1991). Sparse matrix sampling: a screening method for crystallization of proteins. J. Appl. Crystallogr. *24*, 409–411.

Johnson, C.H. (2004). Precise circadian clocks in prokaryotic cyanobacteria. Curr. Issues Mol. Biol. *6*, 103–110.

Jones, T.A., and Kjeldgaard, M. (1997). Electron-density map interpretation. Meth. Enzymol. *277*, 173–208.

Kabsch, W. (1993). Automatic processing of rotation diffraction data from crystals of initially unknown symmetry and cell constants. J. Appl. Crystallogr. *26*, 795–800.

Kageyama, H., Kondo, T., and Iwasaki, H. (2003). Circadian formation of clock protein complexes by KaiA, KaiB, KaiC, and SasA in cyanobacteria. J. Biol. Chem. *278*, 2388–2395.

Katayama, M., Tsinoremas, N.F., Kondo, T., and Golden, S.S. (1999). *cpmA*, a gene involved in an output pathway of the cyanobacterial circadian system. J. Bacteriol. *181*, 3516–3524.

Kitayama, Y., Iwasaki, H., Nishiwaki, T., and Kondo, T. (2003). KaiB functions as an attenuator of KaiC phosphorylation in the cyanobacterial circadian clock system. EMBO J. *22*, 1–8.

Kondo, T., Strayer, C.A., Kulkarni, R.D., Taylor, W., Ishiura, M., Golden, S.S., and Johnson, C.H. (1993). Circadian rhythms in prokaryotes: luciferase as a reporter of circadian gene expression in cyanobacteria. Proc. Natl. Acad. Sci. USA *90*, 5672–5676.

Laskey, R.A., and Madine, M.A. (2003). A rotary pumping model for helicase function of MCM proteins at a distance from replication forks. EMBO Rep. *4*, 26–30.

Leipe, D.D., Aravind, L., Grishin, N.V., and Koonin, E.V. (2000). The bacterial replicative helicase DnaB evolved from a RecA duplication. Genome Res. *10*, 5–16.

Liu, Y., Tsinoremas, N.F., Johnson, C.H., Lebedeva, N.V., Golden, S.S., Ishiura, M., and Kondo, T. (1995). Circadian orchestration of gene expression in cyanobacteria. Genes Dev. *9*, 1469–1478.

Min, H., Liu, Y., Johnson, C.H., and Golden, S.S. (2004). Phase determination of circadian gene expression in *Synechococcus elongatus* PCC 7942. J. Biol. Rhythms *19*, 103–112.

Mori, T., and Johnson, C.H. (2001). Circadian programming in cyanobacteria. Sem. Cell Develop. Biol. *12*, 271–278.

Mori, T., Saveliev, S.V., Xu, Y., Stafford, W.F., Cox, M.M., Inman, R.B., and Johnson, C.H. (2002). Circadian clock protein KaiC forms ATP-dependent hexameric rings and binds DNA. Proc. Natl. Acad. Sci. USA *99*, 17203–17208.

Nakahira, Y., Katayama, M., Miyashita, H., Kutsuna, S., Iwasaki, H., Oyama, T., and Kondo, T. (2004). Global gene repression by KaiC as a master process of prokaryotic circadian system. Proc. Natl. Acad. Sci. USA *101*, 881–885.

Nicholls, A., Bharadwaj, R., and Honig, B. (1993). GRASP: graphical representation and analysis of surface properties. Biophys. J. *64*, 166–170.

Nishiwaki, T., Iwasaki, H., Ishiura, M., and Kondo, T. (2000). Nucleotide binding and autophosphorylation of the clock protein KaiC as a circadian timing process of cyanobacteria. Proc. Natl. Acad. Sci. USA *97*, 495–499.

Otwinowski, Z., and Minor, W. (1997). Processing of X-ray diffraction data collected in oscillation mode. Meth. Enzymol. *276*, 307–326.

Sanner, M.F., Olson, A.J., and Spehner, J.C. (1996). Reduced surface: an efficient way to compute molecular surfaces. Biopolymers *38*, 305–320.

Singleton, M.R., Sawaya, M.R., Ellenberger, T., and Wigley, D.B. (2000). Crystal structure of T7 gene 4 helicase indicates a mechanism for sequential hydrolysis of nucleotides. Cell *101*, 589–600.

Story, R.M., Weber, I.T., and Steitz, T.A. (1992). The structure of the E. coli recA protein monomer and polymer. Nature *355*, 318–325.

Taniguchi, Y., Yamaguchi, A., Hijikata, A., Iwasaki, H., Kamagata, K., Ishiura, M., Go, M., and Kondo, T. (2001). Two KaiA-binding domains of cyanobacterial circadian clock protein KaiC. FEBS Lett. *496*, 86–90.

Terwilliger, T.C. (1997). Maximum likelihood density modification. Meth. Enzymol. *276*, 530–537.

Tong, L., and Rossmann, M.G. (1990). Rotation function calculations with GLRF program. Acta Crystallogr. A *46*, 783–792.

Toth, E.A., Li, Y., Sawaya, M.R., Cheng, Y., and Ellenberger, T. (2003). The crystal structure of the bifunctional primase-helicase of bacteriophage T7. Cell *12*, 1113–1123.

Uzumaki, T., Fujita, M., Nakatsu, T., Hayashi, F., Shibata, H., Itoh, N., Kato, H., and Ishiura, M. (2004). Role of KaiA functional domains in circadian rhythms of cyanobacteria revealed by crystal structure. Nature Struct. Mol. Biol. *11*, 623–631.

Vakonakis, I., Sun, J., Wu, T., Holzenburg, A., Golden, S.S., and LiWang, A.C. (2004). NMR structure of the KaiC-interacting C-terminal domain of KaiA, a circadian clock protein: implications for the KaiA-KaiC interaction. Proc. Natl. Acad. Sci. USA *101*, 1479–1484.

VanLoock, M.S., Yu, X., Yang, S., Lai, A.L., Low, C., Campbell, M.J., and Egelman, E.H. (2003). ATP-mediated conformational changes in the RecA filament. Structure *11*, 1–20.

Williams, S.B., Vakonakis, I., Golden, S.S., and LiWang, A.C. (2002). Structure and function from the circadian clock protein KaiA of *Synechococcus elongatus*: a potential clock input mechanism. Proc. Natl. Acad. Sci. USA *99*, 15357–15362.

Xu, Y., Mori, T., and Johnson, C.H. (2003). Cyanobacterial circadian clockwork: roles of KaiA, KaiB, and the *kaiBC* promoter in regulating KaiC. EMBO J. *22*, 2117–2126.

Ye, S., Vakonakis, I., Ioerger, T.R., LiWang, A.C., and Sacchettini, J.C. (2004). Crystal structure of circadian clock protein KaiA from *Synechococcus elongatus*. J. Biol. Chem. *279*, 20511–20518.

Yu, X., and Egelman, E.H. (1997). The RecA hexamer is a structural homologue of ring helicases. Nat. Struct. Biol. *4*, 101–104.

Accession Numbers

Coordinates have been deposited in the Protein Data Bank under PDB ID code 1TF7.